Short Communication

Assessing the potential of syn-rift sediments for geochronological dating and its implications for the development of Makanjira-Shire basin in south Malawi Rift

Zuze Dulanya [a,*], Aayush Srivastava [b], Tim C. Kinnaird [b], Blackwell Manda [a], Dalitso Kafumbata [a], Edister Jamu [a], Alick Bwanali [a], Winford Masanjala [a]

[a] *University of Malawi, P.O. Box 280, Zomba, Malawi*
[b] *School of Earth and Environmental Sciences, University of St Andrews, Malawi*

A B S T R A C T

The Upper Shire River basin, located within the zone of progressive interaction and linkage between the southern Malawi Rift and Shire Rift Zone, East Africa, presents an early-stage rift setting where rapid denudation processes take place and have profound influence on the geomorphological evolution of the region. The basin is key to the understanding of mechanisms involved in propagation and growth in young rifts. Although the tectonics in the region are well studied, lack of age constraints due to well-dated strata poses challenges in the understanding of the timing and mechanisms of rift evolution in this section of the south Malawi Rift.

We used syn-rift sediments deposited from the rift shoulders to test the applicability of OSL and radiocarbon dating techniques in a poorly dated data-constrained region of the Malawi Rift.

Our results suggest that proper sampling strategy is paramount in using the OSL technique for dating in areas of high dosage such as the one under consideration. However, the technique offers potential for use in these areas. Furthermore, we conclude from these findings that the evolution of the Upper Shire basin was triggered by tectonic movements along the Makongwa scrap that were responsible for redirecting the Likwenu River into the in the Zomba Graben through the Upper Shire at least during the Upper Pleistocene.

1. Introduction

Scarp regions, as key geomorphic and tectonic landforms, can be useful to disentangle climate variability and denudational processes associated with erosion in hinterlands and accommodation in areas of sediment accumulation (Allen and Houvis, 1998; Allen and Densmore, 2000). This is because these geomorphological features function as an architectural element that provides a bridge between the catchment and the sedimentary basin together with its depositional environments (e.g. Rohais et al., 2008; Pederson et al., 2001). Together with their associated sedimentary deposits, the scarps record a region's geological and geomorphological history and may therefore be useful as a means to test ideas about the linkages between deposition, tectonism and climate (Lustig, 1965; Christenson and Purcell, 1985; Dorn et al., 1987; Bull, 1991; Harvey et al., 1999; Rohais et al., 2007; Rohais et al., 2016). This linkage between morpho-tectonics and climate dynamics could be vital for a greater understanding of climate-landscape relationships (Knight et al., 2016; Key et al., 2015; Moore et al., 2007; Nugent, 1990).

Rapid denudation processses, lack of pronounced sedimentary basins and existence of well-developed and dateable sedimentary units for stratigraphic reconstructions in the Middle Shire area pose some key challenges in understanding how young sections of the rifts develop (Dulanya, 2017). Supported by advances in the field of geochronology, techniques such as optically stimulated luminescence (OSL) dating are some of the most promising tools for determining the absolute ages which are useful for the understanding of Neogene to Quaternary environmental processesin these regions (Soares et al., 2010).

However, the potential for the use of OSL and other emerging techniques to date sediments in this region has not been tested despite the occurrence of various sedimentary deposits associated with hillslope and drainage processes in the southern Malawi Rift, particularly the Makanjira-Shire basin (Chapola and Kaphwiyo, 1992). The basin possesses some unique sedimentary deposits in form of pillars or hoodoos (Thornbury, 1969) locally named as the Malape or Chikala pillars.

Hoodos are sculpted geological formations due to differential erosion and weathering between soft and hard rock layers resulting in the formation of topographic landforms with peculiar shapes. The process of weathering leaves a cap of the hard rock that remains to protect a cone of the soft layer below resulting in the formation of a hoodoo is formed (Wang, 2005). These deposits could be significant for the assessment of Neogene-Quaternary paleo-environmental history within this section of the Malawi Rift due to their setting near the rift scarp, and their depositional characteristics,

The aim of this study is to evaluate the potential of Malape sediments for dating the syn-rift sediments for the better understanding of the evolution of the Makanjira-Shire basin within the south Malawi Rift. These sedimentary units mantle part of the Makanjira-Shire basin area near Liwonde (Fig. 1c) and record depositional processes operating across a diverse geological and geomorphical substrate that includes crystalline basement rocks and Mesozoic alkaline intrusive rocks. We used a range of techniques to compare and validate our findings including field geological observations supported by dates obtained using OSL dating technique and a single radiocarbon date obtained from a sedimentary unit within the study area. As described here, the sediments offer a rich record for documenting sedimentation processes linked to the paleo-environmental conditions in the areas surrounding this region.

2. The study area

2.1. Location

The area is found within the Makanjira-Shire basin (Chapola and Kaphwiyo, 1992) of the Malawi Rift situated at southern part of the western branch of the East African Rift System (EARS) and bordered by latitudes 15° 5′ S and 15° 7′ S and by longitudes 35° 20′ E and 35° 23′ E (Fig. 1a, b, c, d).

2.2. Geology of the study area

Proterozoic hornblende-biotite gneiss forms the crystalline basement complex of the study area and is intruded by the E-W trending Chikala-Mongolowe ring complex of upper Jurassic-lower Cretaceous age (Wooley, 2001; Bloomfied, 1965, Fig. 2). This is a suite of alkaline rocks ascribed to the Chilwa-Alkaline Province complex consisting of nepheline syenites and associated minor intrusions such as foyaites and lamprophyres that are assigned to the Chilwa Alkaline Province (Bloomfied, 1965; Wooley, 2001).

Post-basement faulting associated with the development of the Malawi Rift was responsible for the geomorphological development of most of the region and recent sediment deposition along the major drainage basins. In the study area, the crystalline rocks are truncated by the NE-trending Makongwa Scarp, which marks the eastern boundary of the half-graben system defining the eastern arm of Lake Malawi rift zone (Bloomfied, 1965; Manyozo et al., 1984; Dulanya, 2017). The fault throw is greatest at its south-western end near the foot of the Chikala-Mongolowe ring complex (Fig. 2) and decreases in the north-eastern direction. The Makongwa Fault was described as a recent addition of the main boundary faults (Dixey, 1939) in the Shire-Makanjira basin (Chapola and Kaphwiyo, 1992) as denoted, among other things, by presence of triangular facets on the northern slopes of the ring complexes which attest to recent tectonic movements.

This area of the southern Malawi Rift lies at northern-end of the Zomba Graben (Wedmore et al., 2020a/b) and is currently accommodating 0.5–2 mm/yr ENE-WSW-oriented extension between the Rovuma and San Plates (Stamps et al., 2018; Wedmore et al., 2020a).
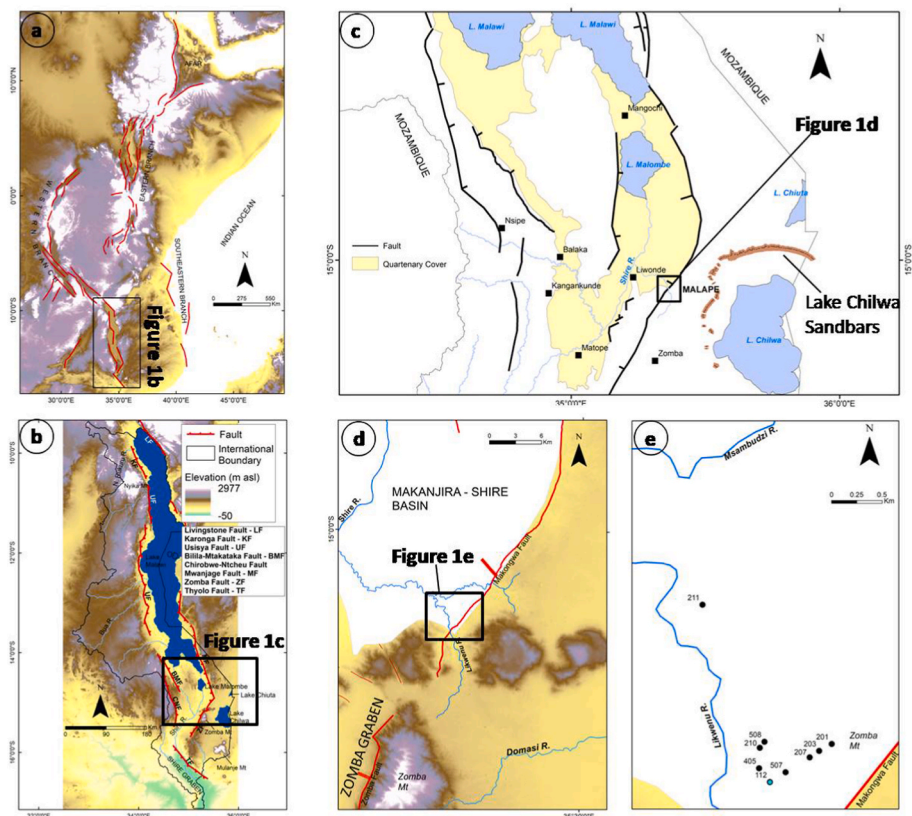
Fig. 1. The location of Malawi on the African continent (a) with the main tectonic features (adopted from Chorowicz, 2005); The Malawi Rift (b) overlaid on an 30m-resolution SRTM DEM showing the main geomorphological and tectonic features; The major drainage and tectonic features of the Makanjira-Shire basin (c) The study area (d) and the study area showing sample locations described in the text (e).
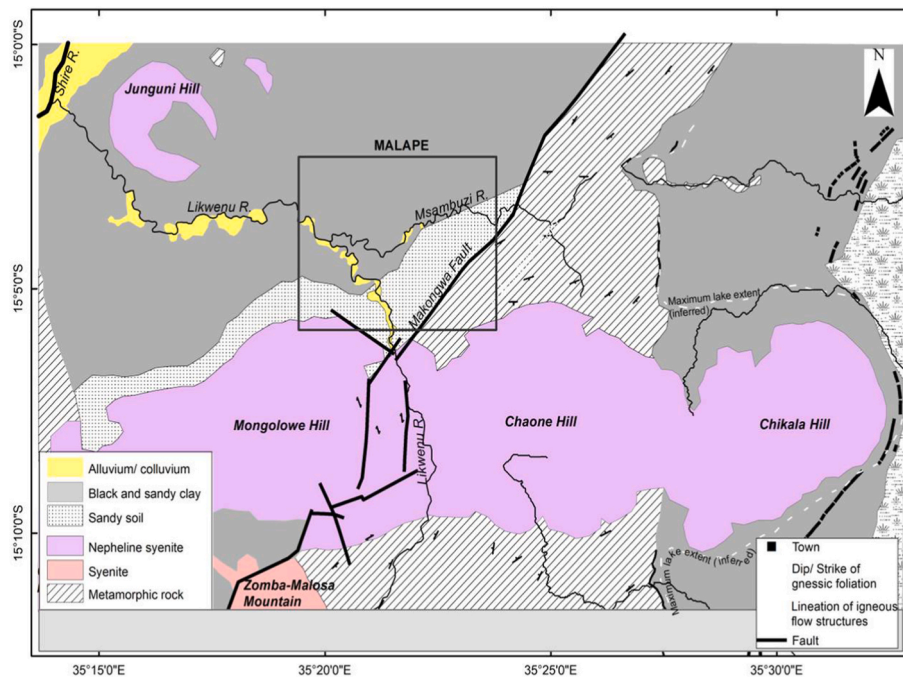
Fig. 2. The geology of the Zomba within the vicinity of the Likwenu River where the Malape Pillars are located (modified after Bloomfied, 1965; Garson, 1960; Manyozo et al., 1984).

Various syn-to post-rift sediments of different origins were deposited in these sub-basins (Bloomfied and Garson, 1965; Bloomfied, 1965). Large parts of both the Shire and the Lake Chilwa Plain study area are covered by superficial cover including black sandy or pale brown and black sandy clays of alluvial/colluvial origin and pediments (Bloomfied and Garson, 1965; Bloomfied, 1965).

2.3. Geomorphology

The geomorphology of the region, just like elsewhere in southern Africa, reflects the long term cyclical tectonic and climatic changes that have affected the region over long time scales (Knight et al., 2016). The Post-Gondwana (Cretaceous age) and the Quaternary peneplanation erosional events (Dill et al., 2005; Lister, 1967) are well represented in the study area (Fig. 3). Escarpments, which are areas characterised by steep gradients lie between the Post-Gondwana and the Quaternary peneplanation erosional surfaces.

2.3.1. Post-Gondwana surface

This surface is preserved along the summits of the ring complexes, rising from 750 m in the Chikala-Mongolowe Hills to over 1000m in the Zomba-Malosa mountains. It consists of undulating plateau surfaces, gently sloping areas and peaks.

2.3.2. Escarpments

These are steep-sided rock cliffs on the sides of the post-Gondwana surfaces. In areas where recent tectonic movements have taken place such as in some areas of Makongwa Scarp, triangular facets are present. In the study area, this surface includes the Domasi and Mlomba Uplands (Fig. 3) considered to have been split from the old valley floor that connected Lakes Chilwa and Malombe by the recent faulting (Dixey, 1939).

2.3.3. Quaternary surfaces

These are either erosional or depositional surfaces that are well-developed at the foot of thescarp.

The Shire Plain which forms part of the Makanjira-Shire basin, is an area on both sides of the Shire River at c. 470–570 m asl formed by
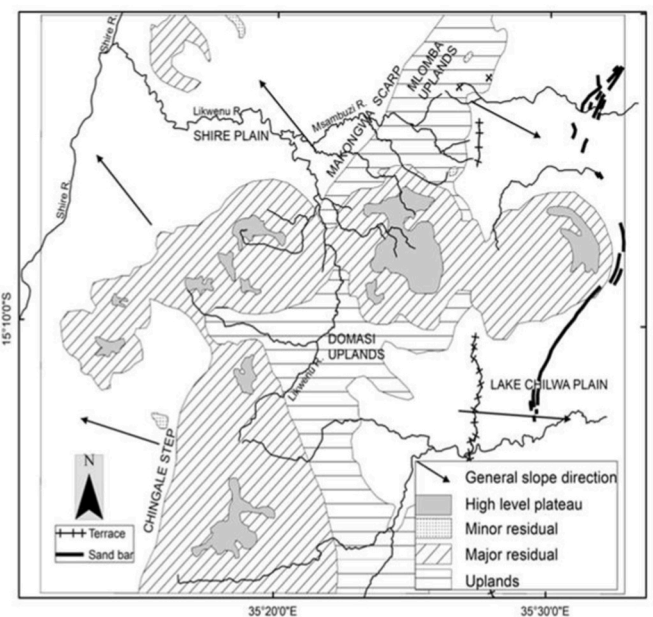
Fig. 3. The geomorphology of the Malape Area (after Bloomfield and Young, 1961; Bloomfied, 1965).

recent faulting and mostly marked on both edges by scarp features. The study site (Malape) which is at ca. 475 m elevation at the toe of the Makongwa Scarp and near the base of the ring complexes is one example of the Quaternaty surface.

The Lake Chilwa Plain is a Miocene surface at about 640–740 m asl consists of an area that gently dips to the east from the Mlomba Uplands in the north and the Shire Highlands to the South. The plain has various terrace features and sand bars that indicate former levels of Lake Chilwa (Garson, 1960).

2.4. Hydrology and climate

The Likwenu and its tributary the Msambuzi River are the main drainage features (Fig. 2b) which flow from the Chikala-Mongolowe Hills and the Mlomba Uplands respectively into the Shire River to the west. The Likwenu River rises from the Zomba Mountain and flows towards the east before it takes a sharp turn to the north and northwest through the scarp regions. It is presumed to have previously flowed into Lake Chilwa but its flow was redirected westward into the Shire River system via drainage capture (Bloomfied, 1965), probably as a result of tectonic activity along the Makongwa Fault.

Climate in the region is largely influenced by the seasonal migration and intensity of the Intertropical convergence zone (ITCZ), caused by tropical high pressure belts over both the Indian and Atlantic Oceans (Nicholson, 2001; Nicholson et al., 2014) and the Congo Air Boundary (CAB) (Abram et al., 2007; Saji et al., 1999).

Malawi's rainfall is variable depending on altitude from 600 mm/a on the rift valley floors to 1600 mm/a in mountainous areas (Nicholson et al., 2014). Temperatures are cool and dry season between May and October with mean temperatures of around 13 °C between June and July; hot and wet November and April with mean temperatures between 30 and 35 °C.

General circulation models show that the African climates are highly sensitive to high latitude glaciations (de Menocal, 1995; Gasse et al., 2008; Clark et al., 2009; Stone, 2014). The Pleistocene-Holocene climates generally show a succession of wet-dry cycles driven by global and regional circulation of various patterns and intensities (e.g. Gasse, 2000; Filippi and Talbot, 2005). There is evidence of wet conditions in the region before the LGM, which was dry, and a wet late glacial, in the region based on lake high stands (Thomas et al., 2009). Similarly, three wet episodes are also documented between early and mid-Holocene time (Boxclaer et al., 2012).

3. Methodology

3.1. Sample collection

Limited field traverses were made from the footwall to the hanging wall of the Makongwa Fault along the assumed transport direction of the sediments to observe the field and stratigraphic relationships of the outcrop to support the observations from the dating techniques described in §3.2. Standard sedimentological and field mapping techniques (e.g. Tucker, 1994) were used to document the Malape Beds and the pillars. Exposed sedimentary sections were logged and all informative properties such as colour, composition, grain size and sorting, matrix content, sedimentary structures, paleoflow directions from the orientation of cross beds, geometrical relationships of stratal surfaces and fossils (if any). Quantitative grain sizes determinations were made after the samples were lightly crushed using a pestle and mortar and sieved rough various mesh sizes. Grain sizes were described and classified using schemes by Folk and Ward (1957).

To assess the applicability of luminescence dating, three samples (CERSA 405, 507 and 508) representing the various parts of the stratigraphy (Fig. 1b/c) were collected by 2.5 cm diameter, 40 cm long light-proof pipes from intact pillars showing sub-horizontal sand and granule stratigraphy in 3-dimensions. These sample points were chosen as representative of the minimum ages of each stratigraphic unit and therefore useful for the interpretation of the depositional ages of the strata. Additionally, a sample MAL1 collected from an outcrop that contained plant remains after excavating approximately 10 cm into one of the eroded hoodoo faces. This sample is considered to be co-eval or younger than the clayey material within which it is found and is the only biogenic sample from the area. Apart from its use in paleoenvironmental interpretations, sample MAL1, would therefore prove useful in validating the ages obtained from the OSL data.

3.2. Geochronological investigations

Samples were prepared and assessed for their potential for luminescence dating, in subdued orange-light conditions at the luminescence laboratories at the School of Earth and Environmental Sciences, University of St Andrews. Prior to preparation of sediment for equivalent dose (D_e) determination, the potentially light-exposed sample tube ends were removed and used for dose rate ($\dot{D}$) measurements. Sediments collected from the central part of the tubes were treated with hydrochloric acid and hydrogen peroxide to remove carbonate and organic materials, respectively and then sieved to isolate 150–250 μm sized fraction. Quartz from samples CERSA 507 and 508 was extracted from the sieved fraction using density separations and 2.62 and 2.70 g/cm^3 using lithium heteropolytungstates in water. Quartz grains were then chemically etched in hydrofluoric acid for 40 min, to remove the alpha-irradiated outer surface of the quartz grains and afterwards treated in fluorosilicic acid (HF) to remove persistent feldspar contamination for three weeks (Srivastava et al., 2019). After each chemical etching, hydrochloric acid was used to remove any fluoride precipitate, and samples were re-sieved to isolate the 150–250 μm sized particles. Sample CERSA 405 did not yield enough quartz so potassium feldspar was extracted from the <2.62 g/cm^3 fraction using density separations at 2.53 and 2.58 g/cm^3 and isolated potassium feldspar grains were not etched in HF to avoid anisotropic removal of the surface. For D_e measurements, prepared quartz and K-feldspar were mounted onto stainless steel discs as a 2 mm (small aliquots) monolayer using Silkospray silicone oil.

D_e measurements were made using Risø DA-20 TL/OSL readers, using the single-aliquot regenerative-dose (SAR) method (Murray and Wintle, 2000). For samples CERSA 507 and 508, an additional stimulation with IR-diodes was added to remove the luminescence signal from any remaining IR-response minerals (e.g. feldspars) prior to stimulation with blue LEDs (post-IR OSL) to measure the quartz OSL signal (Banerjee et al., 2001). For sample CERSA 405, the post IR-IRSL protocol (e.g. Thomsen et al., 2008; Buylaert et al., 2009) was used. Aliquots were included in final D_e calculations when the following rejection criteria were satisfied: (i) recuperation less than 5%; (ii) recycling ratio within 10% of unity, including uncertainties (Murray and Wintle, 2000); and (iii) test dose signals 3σ greater than the background. Final D_e determinations for each sample were based upon at least 20 accepted aliquots. Saturation signals characteristics for samples CERSA 507 and were defined based on two different criteria according to Wintle and Murray (2006).

(i) the natural OSL signal does not intersect with the dose response curve (DRC) and a D_e could be interpolated (Fig. 8a);
(ii) the natural signal interpolates onto the flat, asymptotic part of the DRC at a point that is greater than the 2D$_0$ limit (Fig. 8b). Moreover, interpolation of the natural signal onto the saturated DRC at high doses results in large and asymmetric uncertainty in De (Murray et al., 2002).

For dose rate determinations, radionuclide concentrations (^{232}Th, ^{238}U and ^{40}K) were measured using inductively coupled plasma mass spectrometry (ICPMS) conducted by Activation Laboratories Ltd (Actlabs), Ancaster, Ontario. Infinite matrix dose rates were calculated from these using the conversion factors of Guérin et al. (2011) and were adjusted for attenuation by grain size and chemical etching using the datasets of Guérin et al. (2012) and Bell (1979) respectively, as well as measured moisture content of 4%. Following Prescott and Hutton (1994), $\dot{D}_{cosmic}$ were determined from sample longitude, latitude, altitude, and depth. All dose rate ($\dot{D}$) calculations were made using the DRAC (v1.2) software of Durcan et al. (2015).

Sample MAL1 containing plant remains, was sent for dating to Beta Analytic Radiocarbon Dating Laboratory in Florida (USA) and the ages calibrated to calendar years using the High Probability Density (HPD)

range method (Ramsey, 2009; Hogg et al., 2020).

4. Results

4.1. Geology and stratigraphy

The sediments in the Malape area are dominated by Neogene-Quaternary sediments consisting of poorly consolidated conglomerates and pebbly sandy clays of reddish brown to buff colourson the hanging wall of the Makongwa Scarp.

Grain sizes variations for these sediments generally show a fining decline from the footwall towards the hanging wall and a fining upward sequence from the base of the succession. The proportion of medium and very fine sand is lower near the footwall and increases away from it. The proportion of particles greater than granules initially decreases in the hanging wall but then increases again further out (c. 2 km) from the footwall. These sediments are moderately to poorly sorted and variable in texture and colour (Fig. 4; Table 1).

The sediments generally have flat-lying beds and laminae of variable thickness ranging from a few centimetres to as much as a metre or more. The overall thickness of the beds increases from the footwall into the hanging wall in a general westerly direction. They have the greatest exposure at the area of the Chikala Pillars and some river sections where they attain a maximum thickness of a maximum thickness of c. 9m near the Chikala Pillars (Fig. 5). Elsewhere, they are blanketed by thin soil layers and/or hard pan.

Bedding and bed contacts are poorly developed but overall bedding gets more pronounced westward in the overall sediment transport direction. Apart from the lowermost bed which is dipping to the east (near location 405, Fig. 1e), all the beds are flat lying. Sets and cosets of trough cross-beds are preserved in places and indicate sediment transported basinward, from an east or northeast source. In places, pebble imbrication indicates two general flow directions, one directed west and southwest and another directed northerly (Fig. 6).

The base of this sedimentary succession is dominated by poorly exposed hard variegated reddish brown clay soils that presumably overlie the country rocks. This clay layer is overlain by a thin layer (less than 30 cm) of cobble and boulder-sized unconsolidated conglomerate with angular fragments of largely metamorphic rocks such as gneiss and quartzite and, more rarely, alkaline dykes. The conglomerate layer thins away from the footwall and gives way to a pebble-sized poorly consolidated clayey sediment with an increasing arenaceous component towards its top. The pebbles are dominated by white feldspars with rare fragments of muscovite, biotite and quartz and contain a dark iron coating due to the effect of infiltrating water. The pebbles are marked by a dark iron coating due to the effect of infiltrating water. In the Chikala Pillars area, this unit dips east at 170/30E near the sample location 405 (Fig. 1e and 5; 6a) and becomes increasingly sandy towards its top. At the top of this succession is a pebbly clay layer interbedded with feldpathic conglomerates.

Based on the sediment characteristics described above, we identify two main sediment deposition units. Unit 1 is defined by the conglomerate layer with at the base with sandy-rich sediments derived from metamorphic rocks. Unit 2 at the upper part of the succession which consists of poorly sorted beds with faint bedding planes of mixed sediments in which pale brown and black clay-rich facies and poorly sorted feldspathic pebbly conglomerates of which alkali feldspars are ubiquitous form the topmost part of the succession. Feldspathic conglomerates of poorly sorted reddish-brown sandy clay layers of variable thickness but reaching a maximum thickness of 3m and faint bedding area occasionally found together with plant remains with swamp affinities and animal burrows are present.

4.2. Geochronology

For samples CERSA 507 and 508, natural OSL signals are bright, with relatively fast decays and all measured aliquots passed the rejection criteria (Appendix 1). The OSL signals, Ln/Lx and Rn/Rx were obtained by integrating the OSL counts in the first 1s of stimulation and subtracting an equivalent signal taken from the last 9s (Fig. 7).

Almost all the measured aliquots show characteristics of a saturated signal (92% for CERSA 507 and 96% for CERSA 508). Following Wintle
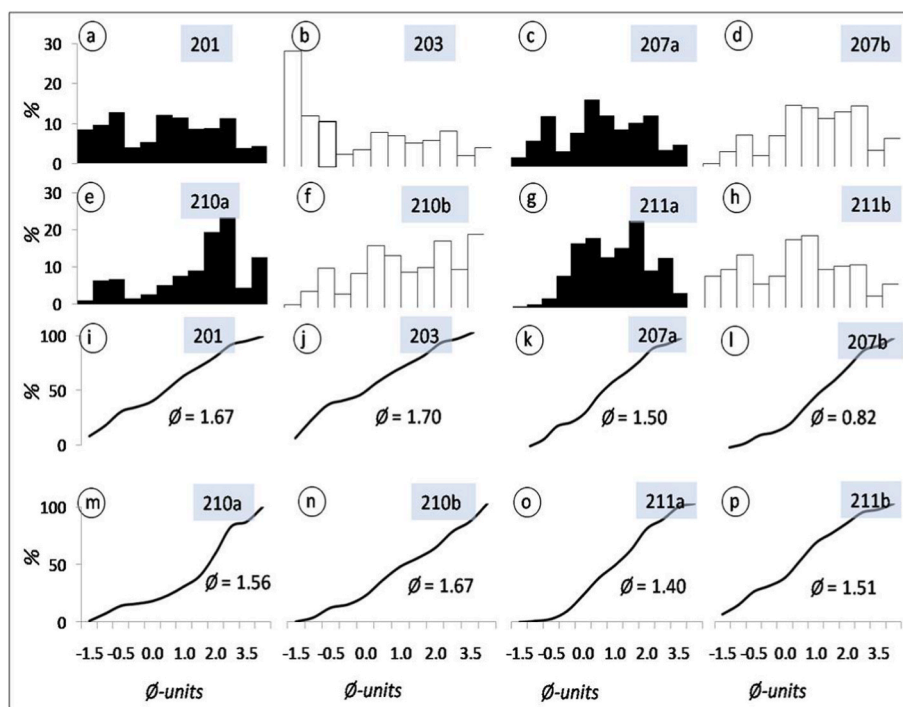
Fig. 4. Grain size histogram distributions (a–h) and cumulative curves (i–p) for sediments measurements from the Malape area. Sorting coefficients (Ø) shown on the cumulative curves are derived from the formula by Folk and Ward (1957).

Table 1
Grain size metrices for various samples collected and shown in Fig. 1e. The sorting and mean values shown are calculated using the phi-scale using formulae by Folk and Ward (1957).

Md(Phi50)	Mean (Phi)	Phi95	Phi5	Phi84	Phi16	Sorting	Class
0.3	0.48	3.75	−1.7	2.25	−1.125	1.67	Poor
−0.5	0.00	3.75	−1.7	2	−1.5	1.70	Poor
0.7	0.80	3.5	−1.12	2.45	−0.75	1.50	Poor
1.25	1.99	3.75	−0.9	2.6	2.125	0.82	Moderate
2	1.62	3.8	−1.125	3.05	−0.2	1.56	Poor
1.49	1.60	4.125	−0.785	3.5	−0.2	1.67	Poor
1.36	1.45	3.625	−0.25	3.125	−0.125	1.40	Poor
0.74	0.62	3.5	−1.7	2	−0.875	1.51	Poor
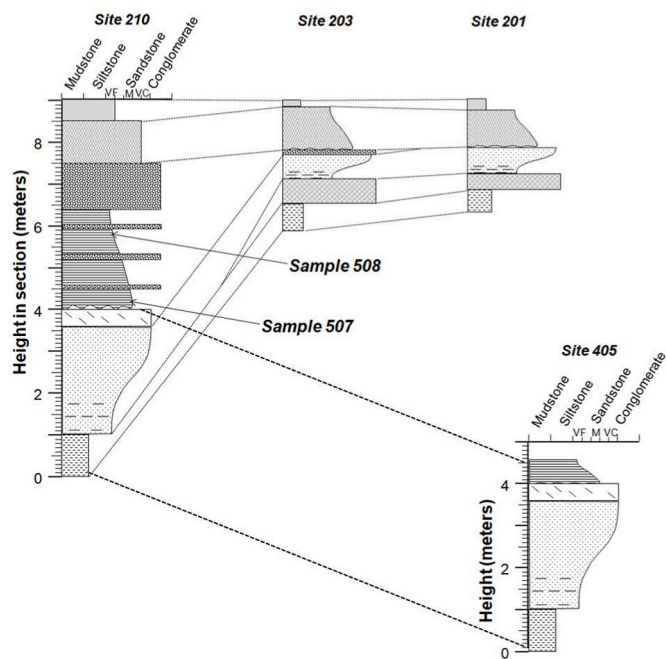
Fig. 5. Stratigraphic sections for sample locations shown in Fig. 1e.

and Murray (2006), D_0 values for each sample was derived from the fitting of the Dose Response Curve (DRC) with a single saturating exponential function

$$I = I_0 (1 - \exp^{-D/D0}) \quad I$$

where I is the OSL intensity after a dose (D), I_0 is the saturation intensity and D_0 is the dose level characteristic of the DRC.

Based on equation I, the upper dating limit for these saturated signals is $2D_0$ (nominally ~85% of the upper saturation point). For the two investigated samples, the D_0 values are between ~65 and 70 Gy, resulting in an upper limit of reliable OSL dating at D_e value of ~140 Gy ($2D_0$), which is comparable to experimental values (e.g. Singarayer and Bailey, 2004; Pawley et al., 2010; Srivastava et al., 2019). Minimum ages have been calculated from the $2D_0$ values reported to the nearest integer and without an uncertainty, reflecting that the 'true' D_e is in excess of quoted minimum (Table 2).
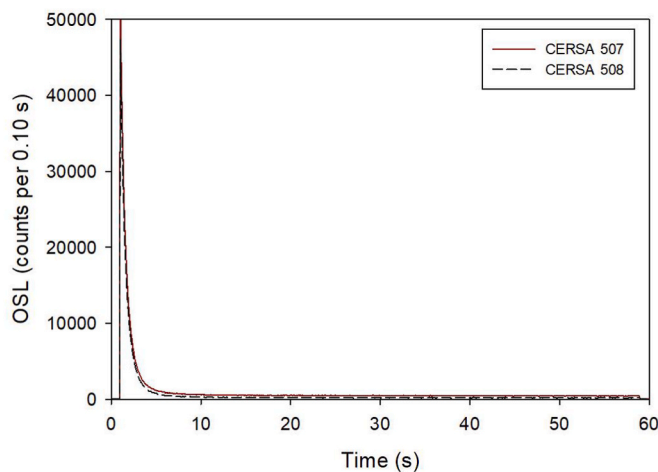
Fig. 7. OSL decay curve shown by an aliquot each of samples CERSA 507 and 508.
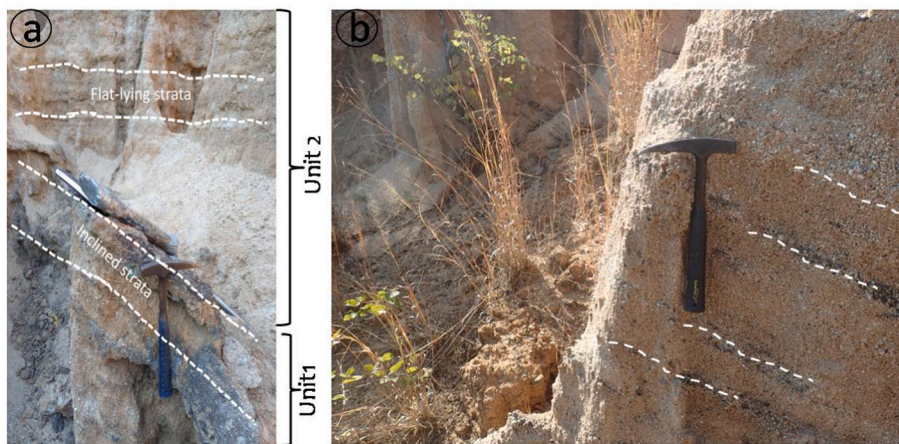
Fig. 6. Some sedimentary structures observed within the sedimentary beds. A dipping cap rock between units 1 and 2 (a) and gently dipping pebbly cross bedded sandstone from unit 1.
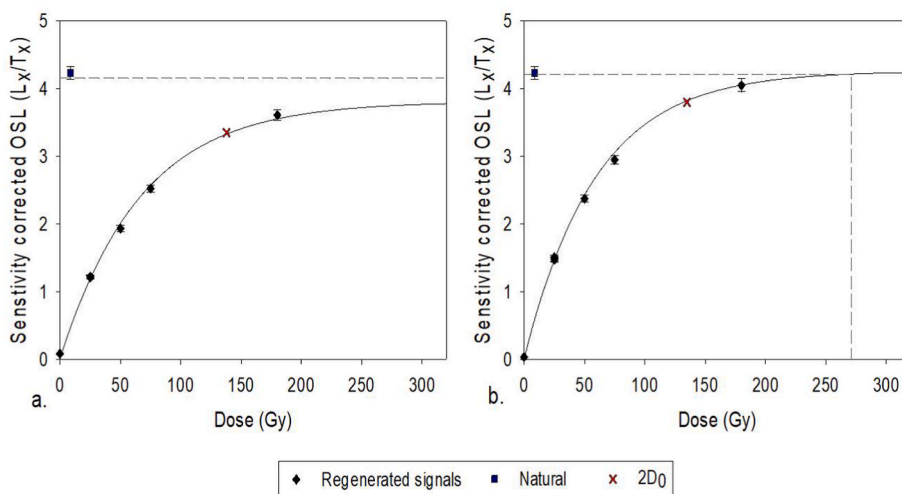
Fig. 8. Examples of two dose response curves from sample CERSA 507 where the natural OSL signal is considered to be in saturation: a) The natural signal does not intercept the dose response curve and b) De exceeds $2D_0$.

The magnitude of dose rates, which is predominantly dependent upon the radionuclide concentrations, are relatively high from the sediments with 3.3–3.5% K, 9.9–10.8 ppm Th and 2.5–3.0 ppm U. The total effective $\dot{D}$ to the Malape Pillar quartz is therefore determined to be ~4.6 Gyka^{-1}. The calculated ages, therefore, fall within the Upper Pleistocene between 28 and 32 ka, which are considered to represent a broad time interval for the Malape sediment depostion.

For sample CERSA 405, IRSL and pIR IRSL environmental dose distributions are wide, implying that the feldspars were poorly bleached at deposition. This is a common quality of grains in fluviatile settings and if the D_e population is dominated by residuals, then led to over-estimations in age. Sub-populations of aliquots trend to a lower apparent dose with a weighted mean of ~33 Gy. This sub-population represents the best-bleached component and is interpreted as yielding a burial dose. The best estimate for deposition of Sample CERSA405 is 5.2 ± 0.8 ka, supported by close agreement in aliquot behaviour distributions and age calculation between IRSL (50 °C) and post-IR IRSL (225 °C) treatments. Post-IR IRSL (290 °C) age estimate is somewhat older though still in the Holocene; but environmental dose distributions of aliquots in this treatment clearly indicate dispersion which probably reflects incomplete bleaching and inheritance of a pre-depositional history.

Results for sample MAL1 indicate a conventional radiocarbon age 9590 ± 30 BP calibrated to approximately 11 Ka (Fig. 9), with d13Corg of −20.1 per mil at both 95% and 68% as shown in Table 3. Except for sample 405, the sample MAL1 indicates a relatively younger age compared to samples 507 and 508. We interpret this to be a post-depositional biological (plant growth) activity in the area prior to the connection of the Likwenu River with the Shire River course.

5. Discussion

5.1. Sedimentation in the Malape basin

The sediments are poorly bedded, sorted and deposited at the foot of
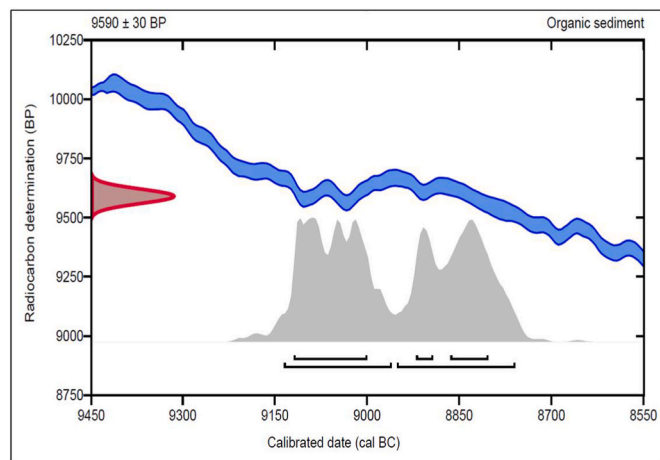
Fig. 9. Calibrated radiocarbon age for sample MAL1.

Table 3
d13C-org of −20.1 per mil at both 95% and 68%.

Probability		Radiocarbon Age	Radiocarbon Age (calendar-calibrated)
95.4%	48.5%	9137 - 8962 cal BC	(11086 - 10911 cal BP)
	46.9%	8953 - 8761 cal BC	(10902 - 10710 cal BP)
68.2%			
	40%	9121 - 9002 cal BC	(11070 - 10951 cal BP)
	19.6%	8866 - 8805 cal BC	(10815 - 10754 cal BP)
	8.7%	8922 - 8895 cal BC	(10871 - 10844 cal BP)

a steep fault scarp and were deposited as as alluvial fan and fluviatile deposits at the base of the Makongwa scarp. The sediment characteristics described above show evidence for rapid deposition (supported by

Table 2
Summary OSL data. Equivalent doses (D_e), dose rates ($\dot{D}$), and ages are shown to two decimal places, with all calculations made prior to rounding. All ages are relative to the year 2021.

Sample	Depth	Discs accepted	D_e	Beta $\dot{D}$	Gamma $\dot{D}$	Cosmic $\dot{D}$	Envir $\dot{D}$	Age
	(m)	(measured)	(Gy)	(Gy.ka^{-1})	(Gy.ka^{-1})	(Gy.ka^{-1})	(Gy.ka^{-1})	(ka)
CERSA 405B	0.5	24 (24)	33.0 ± 4.2	4.09 ± 0.53	1.76 ± 0.2	0.11 ± 0.01	6.36 ± 0.59	5.21 ± 0.80
CERSA 507	3.5	24 (24)	>132.5	2.96 ± 0.26	1.56 ± 0.10	0.14 ± 0.01	4.66 ± 0.28	>28.42
CERSA 508	7	22 (22)	>142.8	2.88 ± 0.24	1.60 ± 0.10	0.10 ± 0.01	4.58 ± 0.26	>31.20

poorly sorted and bedded sediments) into a westward draining basin.

The generalised stratigraphic section of the area (Fig. 10) helps us to infer two main deposition episodes based on compositional variations between unit 1 and 2 demarcated by a dipping bed. This suggests change in sediment provenance during the two episodes. The first depositional episode was associated with the deposition of arenaceous sediments derived largely from the metamorphic basement near the Makongwa scarp derived from the eastern direction. This is supported by mineralogic evidence in the lower units which have affinities to the nearby from the metamorphic basement rock in the eastern part of the area and the orientation direction of the crossbeds. Tectonism along the Makongwa Fault led to the tilting of the sediments on the hanging wall of the fault followed by drainage capture of the Upper Likwenu into the Shire-Makanjira basin (e.g. Bloomfied, 1965; Bloomfield and Young, 1961). The increase in bed thickness from the footwall to the hanging wall also implies fault reactivation may be leading to erosion of the sediments near the footwall.

A wetter climate around the region during the deposition of these sediments is also supported by our age model (28–32 Ka) and OSL ages from the Lake Chilwa sandbars and terraces (Fig. 1c, 2 and 3; Thomas et al., 2009).

5.2. Geochronology

The wide equivalent dose distribution (IRSL and pIR IRSL) observed in sample CERSA405 implies that feldspars were poorly bleached at deposition, consistent with this sediment being deposited in a fluviatile depositional environment. Poor bleaching will lead to over-estimations in age, and an anomalously old, pre-depositional age. As seen from the results, there is a wide geochronological span, ranging from at least c. 26–33 ka to ~5.3 ka. The latter was obtained from a pillar that we suspect was eroded and may therefore be recording recent erosional history in the area following the deposition of the sediments. This coincides with a timespan associated with the onset of an open-basin regime when the Shire River became functional (Rickets and Johnson, 1996). We therefore consider that the c. 26–33 Ka ages are reliable and provide a minimum constraint on the ages of their formation. They are consistent with the proposed age for the Matope Beds within the same basin further south and the proposed timing for the opening of Middle Shire Basin into the lower Shire graben (Bloomfied and Garson, 1965; Dulanya, 2017; Kolawole et al., 2021; Dulanya et al., 2022). The c. 11Ka

radiocarbon age obtained may perhaps reflect an interval in the Upper Pleistocene-Holocene period when there was relative stability and perhaps less erosion and deposition which allowed the allowing for the development of vegetation in a marshy environment (based on the structure of the plant remains observed in the sediments) prior to the Likwenu River's connection with the Middle Shire River.

6. Conclusions

These results suggest that although the dose rate is high in the region due to the peralkaline crystalline basement, with proper sampling strategy and choice of dating technique, it is possible to use the OSL technique to constrain the chronology in this area.

The results show a broad range of values depicting a minimum age of Upper Pleistocene as the time for the Upper Shire basin development and establishment of the upper Shire River section using OSL technique. This time Unit is consistent with other studies in the region (Dulanya et al., 2022, 2017; Kolawole et al., 2021; Rickets and Johnson, 1996). This may support an upper Pleistocene-Holocene opening of the upper Shire (e.g. Rickets and Johnson, 1996; Boxclaer, 2012).

The single Middle Holocene (c. 5.3 Ka) age obtained in this study perhaps reflects recent aggradation such as was reported in the Shire River during the deposition of the Chipalamawamba Beds (Boxclaer, 2012). However, the radiocarbon age (c. 11Ka) does assist in constraining the evolutionary history of this area the transition from aggradation to erosion to be no older than 11 Ka and therefore the Late Pleistocene may be plausible. Despite all these variabilities and uncertainities surrounding the geological and geochronological data, the study indicates that with proper understanding of the region's stratigraphy and a more extensive sampling campaign, the OSL technique could be useful for the dating of the sedimentary sequences present in the South Malawi rift particularly within the Makanjira-Shire basin. The regionmay provideclues for the understanding of the youthful nature of the Upper and Middle Shire river sections and its role in rift evolution and basin growth through processes of tip propagation and segment linkage (e.g. Macleod et al., 2000) which should be the subject of further more detailed studies in the region.

Author statement

ZD and DK devised this study. Field work was led by ZD, DK, EJ, AB,
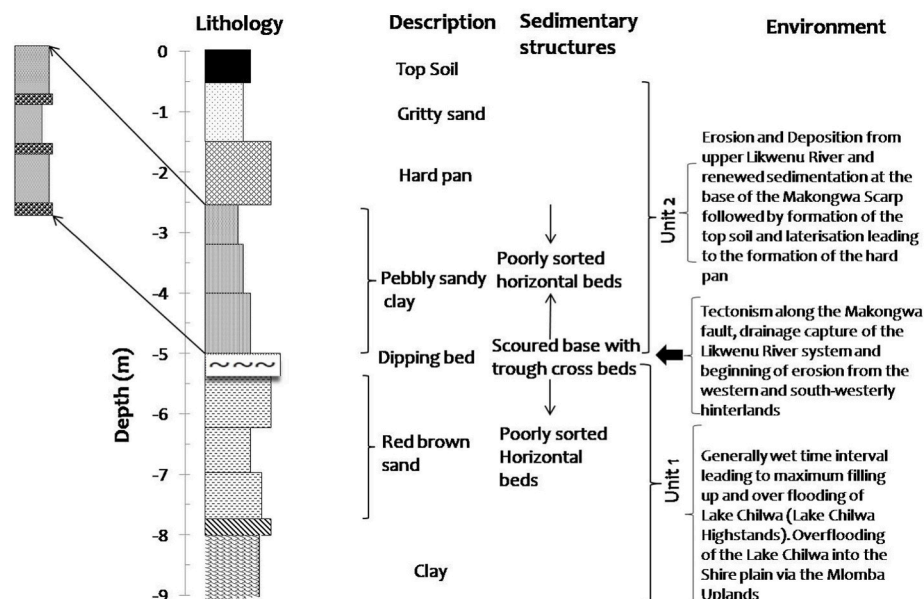
Fig. 10. Generalised stratigraphic section in the Lower Likwenu River near Malape Pillars and a summary of inferred environmental conditions.

BM and WM while data collection and analysis wwas done by ZD, DK, AS and TK. ZD, AS and TK wrote the manuscrpt while all the authors with reviewing this manuscript.

Declaration of competing interest

I, the undersigned, representing the co-authors of the manuscript titled "**Assessing the potential of syn-rift sediments in South Malawi Rift for geochronological dating sediments in parts of the Makanjira-Shire basin"** hereby wish to submit our research work based on our research findings in the area. We hereby declare that:

(a) All the information and statements made in this document are true and we accept that any misinterpretation or misrepresentation contained in this manuscript may lead to our disqualification by publisher.

(b) We have no conflict of interests.

(c) We commit to the ethical standards and publishing guidelines as stipulated by the publisher.

Data availability

No data was used for the research described in the article.

APPENDIX 1

The two growth curves shown in Fig. 8 are representatives for sample CERSA507 (D_0 values for other aliquots for this sample were comparable as shown in the table in appendix 1. CERSA508 had slightly higher D_0 values but adding two more growth curves for this sample will affect the calculated saturation.

	CERSA 507			CERSA 508		
	D0 (Gy)	err (Gy)	2D0 (Gy)	D0 (Gy)	err (Gy)	2D0 (Gy)
Aliquot 1	51.8	1.98	103.6	76.5	3.46	153
Aliquot 2	61.3	2.35	122.6	86.5	4.1	173
Aliquot 3	71.4	2.95	142.8	69.4	3.03	138.8
Aliquot 4	59.2	2.36	118.4	58.7	2.41	117.4
Aliquot 5	73.6	3.02	147.2	64.8	2.8	129.6
Aliquot 6	60.2	2.34	120.4	69.3	2.87	138.6
Aliquot 7	62.1	2.41	124.2	87.3	4.06	174.6
Aliquot 8	64.5	2.62	129	87.7	4.45	175.4
Aliquot 9	63.8	2.54	127.6	66.8	2.91	133.6
Aliquot 10	65.6	2.72	131.2	78.8	3.41	157.6
Aliquot 11	78.6	3.35	157.2	53.6	2.39	107.2
Aliquot 12	66.9	2.69	133.8	79.6	3.6	159.2
Aliquot 13	65.9	2.61	131.8	63.5	2.57	127
Aliquot 14	64.6	2.57	129.2	62.3	2.67	124.6
Aliquot 15	59.1	2.23	118.2	84	3.91	168
Aliquot 16	58.9	2.35	117.8	77.2	3.46	154.4
Aliquot 17	62.7	2.61	125.4	62	2.61	124
Aliquot 18	78.2	3.34	156.4	75.2	3.35	150.4
Aliquot 19	76.9	3.32	153.8	62.1	3.45	124.2
Aliquot 20	66.7	2.74	133.4	71.1	3.4	142.2
Aliquot 21	78.2	3.6	156.4	71.4	3.12	142.8
Aliquot 22	64.6	2.56	129.2	63.6	2.87	127.2
Aliquot 23	68.1	2.75	136.2			
Aliquot 24	66.7	2.66	133.4			

References

Abram, N., Gagan, M., Hantoro, W., McCulloch, M., Chappell, J., Suwargadi, B., 2007. Seasonal characteristics of the Indian ocean dipole during the Holocene epoch. Nature 445, 299–302.

Allen, P.A., Densmore, A.L., 2000. Sediment fluxfrom an uplifting fault block. Basin Res. 12, 367–380.

Allen, P.A., Houvis, N., 1998. Sediment supply from landslide-dominated catchments: implications for basin-margin fans. Basin Res. 10, 19–35.

Banerjee, D., Murray, A.S., Bøtter-Jensen, L., Lang, A., 2001. Equivalent dose estimation using a single aliquot of polymineral fine grains. Radiat. Meas. 33 (1), 73–94.

Bell, W.T., 1979. Attenuation factors for the absorbed radiation dose in quartz inclusions for thermoluminescence dating. Ancient TL 8 (2), 12.

Bloomfied, K., 1965. The geology of the Zomba area. Bull. Geol. Soc. Malays. 16.

Bloomfied, K., Garson, M.S., 1965. The geology of the Kirk Range – Lisungwe Valley Area. Bulletin of the Geological Survey of Malawi 17.

Bloomfield, K., Young, A., 1961. The Geology and Geomorphology of Zomba Mountain. The Nyasaland Journal14, pp. 54–80.

Bull, W.B., 1991. Geomorphicresponsestoclimaticchange. Oxford University Press, New York, p. 326.

Christenson, G.E., Purcell, C., 1985. Correlation and ageofQuaternary-fan sequences, Basin and Range province, southwestern United States. In: Weide, D.L. (Ed.), Soils and Quaternary geology of the southwestern United States: Boulder, Colorado. Geological Society of America Special Paper 203, pp. 115–122.

Chapola, L.S., Kaphwiyo, C.E., 1992. The Malawi Rift: geology, tectonics and seismicity. Tectonophysics 209, 159–164.

Clark, P.U., Dyke, A.S., Shakun, J.D., Carlson, A.E., Clark, J., Wohlfarth, B., Mitrovica, J. X., Hostetler, S.W., McCabe, A.M., 2009. The last glacial maximum. Science 325, 710–714.

De Menocal, P.B., 1995. Plio-pleistocene african climate. Science 270, 53–59.

Dill, H.G., Ludwig, R.R., Kathewera, A., Mwenelupembe, J., 2005. A lithofacies terrain model for the Blantyre Region: implications for the interpretation of palaeosavanna depositional systems and for environmental geology and economic geology in southern Malawi. J. Afr. Earth Sci. 41, 341–393.

Dixey, F., 1939. The early cretaceous valley-floor peneplain of the Lake nyasa region and its relation to tertiary rift structures. Quartern.Geol.Soc. London 116, 255–258.

Dorn, R.I., DeNiro, M.J., Aije, H.O., 1987. Isotopicevidenceforclimaticinfluence on alluvial-fan development in death valley. Geology 15, 108–110.

Dulanya, Z., 2017. A review of the geomorphotectonic evolution of the south Malawi rift. J. Afr. Earth Sci. 129, 728–738.

Dulanya, Z., Gallen, S.F., Kolawole, F., Williams, J.N., Wedmore, L.N.J., Biggs, J., Fagereng, Å., 2022. Knickpoint morphotectonics of the Middle Shire River basin: implications for the evolution of rift interaction zones. Basin Res. 00, 1–20. https://doi.org/10.1111/bre.1268.

Durcan, J.A., King, G.E., Duller, G.A., 2015. DRAC: dose rate and age calculator for trapped charge dating. Quat. Geochronol. 28, 54–61.

Filippi, M.L., Talbot, M.R., 2005. The palaeolimnology of northern Lake Malawi over the last 25ka based upon the elemental and stable isotopic composition of sedimentary organic matter. Quat. Sci. Rev. 24, 1303–1328.

Folk, R.L., Ward, W.C., 1957. A study in the significance of grain size parameters. J. Sediment. Petrol. 27, 3–26.

Garson, M.S., 1960. The geology of the Lake Chilwa area. Bull. Geol. Soc. Malays. 12.

Gasse, F., 2000. Hydrological changes in the african tropics since the last glacial maximum. Quat. Sci. Rev. 19, 189–211.

Gasse, F., Chalié, F., Vincens, A., Williams, M.A.J., Williamson, D., 2008. Climatic patterns in equatorial and southern Africa from 30,000 to 10,000 years ago reconstructed from terrestrial and near-shore proxy data. Quat. Sci. Rev. 27 (25–26), 2316–2340.

Guérin, G., Mercier, N., Adamiec, G., 2011. Dose-rate conversion factors: update. Ancient TL 29 (1), 5–8.

Guérin, G., Mercier, N., Nathan, R., Adamiec, G., Lefrais, Y., 2012. On the use of the infinite matrix assumption and associated concepts: a critical review. Radiat. Meas. 47 (9), 778–785.

Harvey, A.M., Wigand, P.E., Wells, S.G., 1999. Response of alluvial-fan systems to the Late Pleistocene to Holocene climatic transition—contrast between the margins of pluvial lakes Lahontan and Mojave, NV and CA, USA. Catena 36, 255–281.

Hogg, A.G., Heaton, T.J., Palmer, J.G., Turney, C.S.M., Southon, J., Bayliss, A., Blackwell, P.G., Boswijk, G., Ramsey, C.B., Pearson, C., Petchey, F., Reimer, R., Reimer, R., Wacker, L., 2020. SHCal20 southern hemisphere calibration, 0–55,000 Years cal BP. Radiocarbon 62 (4), 759–778.

Key, R.N., Cotterill, F.D.P., Moore, A.E., 2015. The Zambezi River; an archive of tectonic events linked to the almagamation and disruption of Gondwana and subsequent evolution of the African Plate. South African J.Geol. 118 (4), 425–438.

Knight, J., Stratford, D., Grab, S.W., 2016. Landscape–climate–human interactions in southern Africa. In: Knight, J., Grab, S.W. (Eds.), Quaternary Environmental Change in Southern Africa: Physical and Human Dimensions. Cambridge University Press, pp. 412–431.

Kolawole, F., Firkins, M.C., Al Wahaibi, T.S., Atekwana, E.A., Soreghan, M.J., 2021. Rift Transfer Zones and the Stages of Rift Linkage in Active Segmented Continental Rift Systems. Basin Research. https://eartharxiv.org/repository/view/2032/.

Lister, L.A., 1967. Erosion surfaces in Malawi. Records Geol.Surv. Malawi VII 15–28.

Lustig, L.K., 1965. Clasticsedimentation in Deep Springs Valley, California. U.S. Geological Survey Professional Paper 352F, pp. 131–192.

Manyozo, D.M., M'ndala, A.T., Phiri, F.R., 1984. The geology of Lake MalombeArea. Bull. Geol. Soc. Malays. 33.

Moore, A.E., Coterrill, F.P.D., Mian, M.P.L., Williams, H.B., 2007. The zambezi river. In: Gupta, A. (Ed.), Large Rivers: Geomorphology and Management. John Wiley and Sons Ltd, London, pp. 311–332.

Murray, A.S., Wintle, A.G., 2000. Luminescence dating of quartz using an improved single-aliquot regenerative-dose protocol. Radiat. Meas. 32 (1), 57–73.

Murray, A.S., Wintle, A.G., Wallinga, J., 2002. Dose estimation using quartz OSL in the non-linear region of the growth curve. Radiat. Protect. Dosim. 101 (1–4), 371–374.

Nicholson, S.E., 2001. Climatic and environmental change in Africa during the last two centuries. Clim. Res. 17, 123–144.

Nicholson, S.E., Klotter, D., Chavula, G., 2014. A detailed rainfall climatology for Malawi, Southern Africa. Int. J. Climatol. 34, 315–325.

Nugent, C., 1990. The Zambezi River: tectonism, climatechange and drainageevolution. Palaeogeogr. Palaeoclimatol. Palaeoecol. 78, 55–69.

Pawley, S.M., Toms, P., Armitage, S.J., Rose, J., 2010. Quartz luminescence dating of Anglian Stage (MIS 12) fluvial sediments: comparison of SAR age estimates to the terrace chronology of the Middle Thames valley, UK. Quat. Geochronol. 5 (5), 569–582.

Pederson, J., Smith, G., Pazzaglia, F., 2001. Comparing the modern, Quaternary, and Neogene records of climate-controlled hillslope sedimentation in southeast Nevada. Geol. Soc. Am. Bull. 113 (3), 305–319.

Prescott, J.R., Hutton, J.T., 1994. Cosmic ray contributions to dose rates for luminescence and ESR dating: large depths and long-term time variations. Radiat. Meas. 23 (2–3), 497–500.

Ramsey, B.C., 2009. Bayesian analysis of radiocarbon dates. Radiocarbon 51 (1), 337–360.

Rickets, R.D., Johnson, T.C., 1996. Early Holocene changes in lake level and productivity in Lake Malawi as interpreted from Oxygen and carbon isotopic measurements of authigenic carbonates. In: Johnson, T.C., Odada, E.O. (Eds.), The Limnology, Climatology and Paleoclimatology of the East African Lakes. Gordon and Breach, Amsterdam, pp. 475–493.

Rohais, S., Eschard, R., Ford, M., Guillocheau, F., Moretti, I., 2007. Stratigraphic architecture of the Plio-Pleistocene infill of the Corinth Rift; implications for its structural evolution. Tectonophysics 440 (1–4), 5–28.

Rohais, S., Ventra, D., de Boer, P.L., 2008. Quantifying Climatic and Tectonic Forcing of Alluvial-Fan Stratigraphy by 3D Numerical Modeling and Comparison with Outcrop Examples.Search and Discovery Article #40363 (San Antonio, Texas).

Saji, N.H., Goswami, B.N., Vinayachandran, P.N., Yamagata, T., 1999. A dipole mode in the tropical Indian Ocean. Nature 401, 360–363.

Singarayer, J.S., Bailey, R.M., 2004. Component-resolved bleaching spectra of quartz optically stimulated luminescence: preliminary results and implications for dating. Radiat. Meas. 38 (1), 111–118.

Soares, E.A.A., Tatumi, S.H., Riccomini, C., 2010. OSL age determinations of Pleistocene fluvial deposits in Central Amazonia. An Acad. Bras Ciências 82 (3). https://doi.org/10.1590/S0001-37652010000300017.

Srivastava, A., Durcan, J.A., Thomas, D.S., 2019. Analysis of late Quaternary linear dune development in the Thar Desert, India. Geomorphology 344, 90–98.

Stamps, D.S., Saria, E., Kreemer, C.A., 2018. Geodetic strain rate model for the East African Rift System. Sci. Rep. 8, 732. https://doi.org/10.1038/s41598-017-19097-w, 2018.

Stone, A.E.C., 2014. Last Glacial Maximum conditions in southern Africa: are we any closer to understanding the climate of this time period? Prog. Phys. Geogr. Earth Environ. 38 (5), 519–542.

Thomas, D.S.G., Bailey, R., Shaw, A., Durcan, J.A., Singarayer, J.S., 2009. Late Quaternary high stands at Lake Chilwa, Malawi: frequency, timing and possible forcing mechanisms in the last 44 ka. Quat. Sci. Rev. 28, 526–539.

Thornbury, W.D., 1969. Principles of Geomorphology, second ed. John Wiley and Sons, Inc, New York.

Tucker, M.E., 1994. SedimentaryPetrology. Blackwell Scientific Publications, Oxford.

Wedmore, L., Biggs, J., Williams, J.N., Fagereng, A., Dulanya, Z., Mphepo, F., Mdala, H., 2020a. Active fault scarps in southern Malawi and their implications for the distribution of strain in incipient continental rifts. Tectonics. https://doi.org/10.1029/2019TC005834.

Wedmore, L.N.J., Williams, J.N., Biggs, J., Fagereng, Å., Mphepo, F., Dulanya, Z., Willoughby, J., Mdala, H., Adams, B., 2020b. Depth-dependent controls on structure, reactivation and geomorphology of the active Thyolo border fault, Malawi rift. J. Struct. Geol.

Wooley, A.R., 2001. Alkaline rocks and carbonatitesof the World part 3: Africa. Geological Society of London, p. 372.

Wintle, A.G., Murray, A.S., 2006. A review of quartz optically stimulated luminescence characteristics and their relevance in single-aliquot regeneration dating protocols. Radiat. Meas. 41 (4), 369–391.